catalysts

MDPI

Article

# Identification of AHL Synthase in Desulfovibrio vulgaris Hildenborough Using an In-Silico Methodology

**Abhilash Kumar Tripathi [1,2,†], Dipayan Samanta [1,3,†], Priya Saxena [1,4], Payal Thakur [1,4], Shailabh Rauniyar [1,2], Kian Mau Goh [5] and Rajesh Kumar Sani [1,2,3,4,6,*]**

1 Department of Chemical and Biological Engineering, South Dakota School of Mines and Technology, Rapid City, SD 57701, USA
2 2-Dimensional Materials for Biofilm Engineering, Science and Technology, South Dakota School of Mines and Technology, Rapid City, SD 57701, USA
3 BuG ReMeDEE Consortium, South Dakota School of Mines and Technology, Rapid City, SD 57701, USA
4 Data Driven Material Discovery Center for Bioengineering Innovation, South Dakota School of Mines and Technology, Rapid City, SD 57701, USA
5 Faculty of Science, Universiti Teknologi Malaysia, Johor 81310, Malaysia
6 Composite and Nanocomposite Advanced Manufacturing Centre—Biomaterials, Rapid City, SD 57701, USA
* Correspondence: rajesh.sani@sdsmt.edu
† These authors contributed equally to this work.

**Abstract:** Sulfate-reducing bacteria (SRB) are anaerobic bacteria that form biofilm and induce corrosion on various material surfaces. The quorum sensing (QS) system that employs acyl homoserine lactone (AHL)-type QS molecules primarily govern biofilm formation. Studies on SRB have reported the presence of AHL, but no AHL synthase have been annotated in SRB so far. In this computational study, we used a combination of data mining, multiple sequence alignment (MSA), homology modeling and docking to decode a putative AHL synthase in the model SRB, Desulfovibrio vulgaris Hildenborough (DvH). Through data mining, we shortlisted 111 AHL synthase genes. Conserved domain analysis of 111 AHL synthase genes generated a consensus sequence. Subsequent MSA of the consensus sequence with DvH genome indicated that DVU_2486 (previously uncharacterized protein from acetyltransferase family) is the gene encoding for AHL synthase. Homology modeling revealed the existence of seven -helices and six  sheets in the DvH AHL synthase. The amalgamated study of hydrophobicity, binding energy, and tunnels and cavities revealed that Leu99, Trp104, Arg139, Trp97, and Tyr36 are the crucial amino acids that govern the catalytic center of this putative synthase. Identifying AHL synthase in DvH would provide more comprehensive knowledge on QS mechanism and help design strategies to control biofilm formation.

**Keywords:** acyl homoserine lactone; biofilm; docking; homology modeling; multiple sequence alignment; quorum sensing; sulfate-reducing bacteria



**Citation:** Tripathi, A.K.; Samanta, D.; Saxena, P.; Thakur, P.; Rauniyar, S.; Goh, K.M.; Sani, R.K. Identification of AHL Synthase in Desulfovibrio vulgaris Hildenborough Using an In-Silico Methodology. Catalysts **2023**, 13, 364. https://doi.org/10.3390/catal13020364

Academic Editor: Fernando P. Cossío

Received: 30 November 2022
Revised: 27 January 2023
Accepted: 4 February 2023
Published: 7 February 2023



## 1. Introduction

Sulfate-reducing bacteria (SRB) are anaerobic microbes that oxidize an array of organic compounds (lactate, pyruvate, and malate) and hydrogen to reduce sulfate and generate hydrogen sulfide ($H_2S$) [1]. $H_2S$ may then react with iron alloys to produce various iron sulfides e.g., pyrite ($FeS_2$) [2]. The formation of pyrite leads to galvanic coupling between pyrite particles and metal surfaces that leads to localized corrosion [3]. This form of corrosion by $H_2S$ and pyrite is called chemical microbe-induced corrosion (CMIC). However, certain members of SRB induce corrosion by direct uptake electrons from the metal surface using pili, nanowires, and outer membrane redox-active proteins (also known as electrical microbial induced corrosion (EMIC)) [4].

The occurrence of a biofilm matrix can accelerate both CMIC and EMIC. Biofilm creates an anoxic ecological niche in which SRB grows, resulting in localized corrosion

and formation of pits [5]. The quorum sensing (QS) machinery in SRB governs biofilm formation. QS is a cell-to-cell communication system widely used by both gram-positive and gram-negative bacteria to regulate gene expression in response to a wide range of environmental stresses (e.g., osmotic, thermal, heavy metal stress) [6]. QS is a population density-dependent mechanism that is activated only when the QS signaling molecules accumulate to a certain level in response to an external stress [7]. QS regulatory networks are very complex and comprise several genes whose products affect biofilm formation. QS signal molecules belong to a wide range of chemical classes, including acyl homoserine lactones (AHLs), boron-furan-derived signal molecules (auto-inducer 2 (AI2)), cis-unsaturated fatty acids (DSF family signals), and small peptides [8,9].

Most of the gram-negative SRB have been reported to secrete several AHL QS molecules [10–12]. Decho and Visscher found different carbon chain AHL molecules (C4 to C14) in microbial mats with a high abundance of SRB [13]. Literature also reported the presence of several AHL molecules (C6-AHL, oxo-C6-AHL, C8-AHL, C10-AHL, and C12-AHL) by SRB isolate Desulfovibrio strain H2.3jLac [14]. These observations clearly indicate the presence of molecular machinery for the synthesis of AHLs in a diverse group of SRB. AHL molecules comprise of an acyl group and a homoserine lactone ring. The acyl group is transferred by the acyl carrier protein (acpP) to the -amino group in S-adenosyl-L-methionine (SAM) [15].

AHLs may be saturated or unsaturated and primarily vary with respect to length of C-atoms (C4 to C18). The acyl group can be a straight chain or altered at the C-3 location by a double bond, an oxo group, or a hydroxyl group. The homoserine lactone ring is N-acylated at the C-1 position, with a fatty acyl group ranging from 4 to 18 carbons [14]. These AHL molecules are secreted out of the cell either by passive diffusion or by a combination of diffusion and active efflux [16]. At a threshold level that depends on the bacterial population, AHL molecules interact with specific transcription factors such as LuxR or LuxR-homologs. The transcription factor-AHL complex binds to specific promoter sequences in the genome to regulate gene expression, resulting in various phenotypic traits e.g., biofilm formation [17].

Our group recently identified various homologs of QS genes in different SRB [18]. Genome mining of SRB genomes revealed the presence of various QS proteins homologous to LuxR, LuxP, LuxQ, and LuxO in different Desulfovibrio spp. These QS proteins are transcriptional regulator proteins that alter gene expression in the presence of AHL QS molecules. The genome of Desulfovibrio vulgaris Hildenborough (DvH) contains the genes that encode for the homologs of proteins LuxR and LuxO [18]. LuxO is a two-component response regulator that acts as a coordinated switch and regulates biofilm formation [19]. LuxO is activated at low cell density and, together with sigma factor (54), induces the transcription of small regulatory RNAs (sRNAs) [20]. These sRNAs act together with the RNA chaperone (HFq) to destabilize and degrade mRNA of another QS protein, LuxR, that regulates QS phenotype, such as biofilm formation [21,22]. However, at high cell density, QS molecules such as AHL reach higher concentrations that results in dephosphorylation and inactivation of LuxO. Activator protein LuxR, an AHL signal molecule receptor transcription factor, activates and induces the expression of genes responsible for various phenotypic traits, including biofilm formation [22,23]. A figurative depiction QS system involving AHL molecules is shown in Figure 1.

As DvH contains AHL receptor transcription factors such as LuxR and QS AHL molecules, we hypothesize the presence of AHL synthase gene in it. To the best of our knowledge, no study has reported the presence of a specific AHL synthase in DvH. A combination of data mining, MSA, and mechanistic and structural studies were used to identify DvH AHL synthase and provide insights into its substrate specificity. Identification of AHL synthase in DvH could provide a better understanding of QS mechanism and establish a molecular framework to establish QS inhibition strategies that prevent AHL signal synthesis and thereby avert biofilm formation. The prevention of QS signal and

thereby biofilm formation is critical for developing therapeutic strategies against infectious microorganisms, and for the prevention of metal corrosion by SRB.

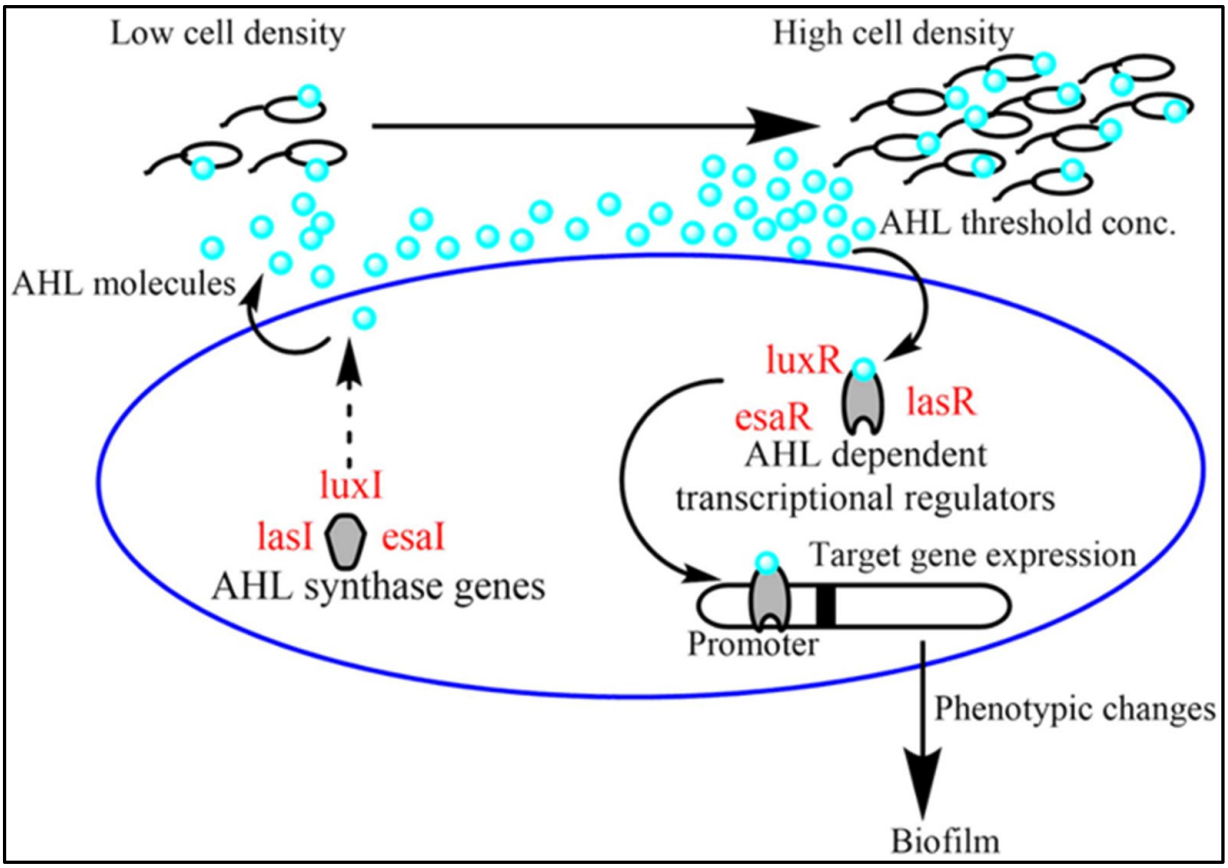


**Figure 1.** Mechanism of QS system in gram-negative bacteria involving AHL molecules.

## 2. Results and Discussion

### 2.1. Data Mining and Prediction of AHL Synthase Using Multiple Sequence Alignment

The complete collection of AHL synthase genes and corresponding protein sequences were sourced from UniProtKB. After filtering based on molecular function (N-acyl homoserine lactone synthase activity) and biological process (quorum sensing), 111 AHL genes were selected for further processing. The AHL synthase gene frequency (number of organisms sharing a particular AHL synthase gene) is shown in Figure 2. The figure shows only those genes which were present in more than five organisms. The RAST genome annotation resulted in 974 uncharacterized proteins in genome of the DvH. Multiple sequence alignment (MSA) was performed between the annotated genome and the 111 AHL synthase proteins to develop a similarity matrix using the DECIPHER Package in R programming language. All the uncharacterized proteins were filtered based on protein sequence length (170 aa to 225 aa) and similarity (%) (>20%) [24], which provided 61 uncharacterized proteins (includes the domain-containing proteins). These shortlisted protein sequences were then subjected to MSA with the consensus sequence-derived ORF. Finally, we narrowed down on the most probable AHL synthase in DvH that has the synthase/transferase motif as in 111 AHL synthase gene. The gene ID for this probable AHL synthase protein in DvH was DVU_2486 (UniProt Id–Q728W6). To validate the function and to understand the arrangement of active site and substrate specificity, we modeled the structure of the DvH AHL synthase using molecular docking, as discussed below.

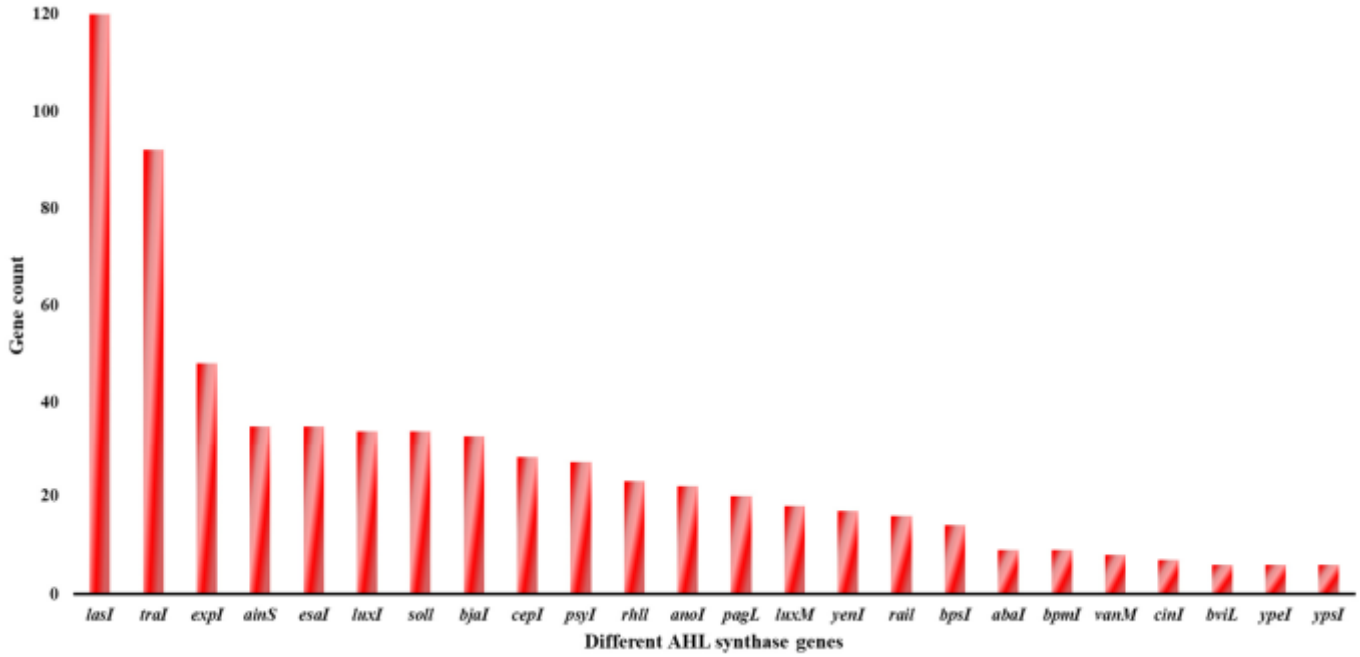


**Figure 2.** Number of organisms sharing an AHL synthase gene. The X-axis denotes the frequency of organisms in a particular AHL gene, and the Y-axis denotes the gene names for the AHL syn-thase present in those organisms. A brief description of the genes listed in Y-axis are provided in Table S1 [25–50].

### 2.2. Modeling of AHL Synthase of Desulfovibrio vulgaris Hildenborough

The identity, query coverage, and E-value of modelled AHL synthase structure with the PDB ID #6EDV were 50%, 96%, and 1.2 10 $^{51}$, respectively. Thus, #6EDV was used as the template AHL synthase. Modeling of the AHL synthase structure from DvH resulted in 20 different models with different DOPE scores, but the same GA341 score (=1.0000). Amongst all AHL synthase models, the structure with the minimal DOPE ( 20941.3925) and GA341 score of 1.0000 was taken as the best model. The energy-minimized structure and dope score per residue of AHL synthase are shown in Figure 3a,b, respectively. The DOPE score per residue was plotted against the amino acid position for both the template structure (#6EDV) and the protein model generated using Modeler. The DOPE score per residue demonstrates the geometrical stability of a specific region within the secondary structure of protein. The minimum DOPE score per residue of the modeled structure as compared to the template structure indicates more stability in the secondary structure.

The Ramachandran plot for AHL synthase modeling is shown in the supplementary information (Figure S1). Stereochemical analysis depicted that the percentage of residues for AHL synthase in the favorable region of the modeled structure was 97.21%, and Ramachandran outliers were 0% (Table S2). Other stereochemical characteristics for AHL synthase can also be found in Table S2. The RMSD between the AHL synthase and the template (#6EDV) was 0.214 Å. High percentages of residues in the favorable region and less RMSD values indicate an excellent geometry of the modeled protein structure. The sequence alignment and superimposition between the modeled AHL synthase and the template structures are shown in Figure S2.

The model confidence of the AlphaFold (Identifier: AF-Q728W6-F1, position 1–181) of DVU_2486 was found to be >90 pLDDT (per-residue confident score). We compared structures of our modelled AHL synthase and predicted AlphaFold with the aid of two parameters: (1) DOPE score per residue and (2) RMSD (root mean square deviation). The DOPE scores per residue of 181 amino acid residues from both the AlphaFold and the modeler-based structures were statistically analyzed based on the null hypothesis principle using the t-test in Microsoft Excel 365 (shown in Table S3) [51]. The mean DOPE scores

per residue of the AlphaFold and the Modeler structure in the t-test were 0.04155 and 0.04092, respectively, and the variances were 2.13 10 $^{5}$ and 2.11 10 $^{5}$, respectively. In the paired unequal variance t-test, the p-value for two-tailed t-test (0.195) is much higher than the value of alpha chosen (0.05); therefore, the null hypothesis cannot be rejected. No significant differences between the DOPE per residue score of the two models were observed. Furthermore, the RMSD between the predictive AlphaFold- and modeler-based models was 0.746 Å, and the superimposition is shown in Figure S3. The superimposition suggests that the folding of -helices and the turns for the sheets have no significant difference. The overall modeler-based structure coincides with the predictive structure from AlphaFold.

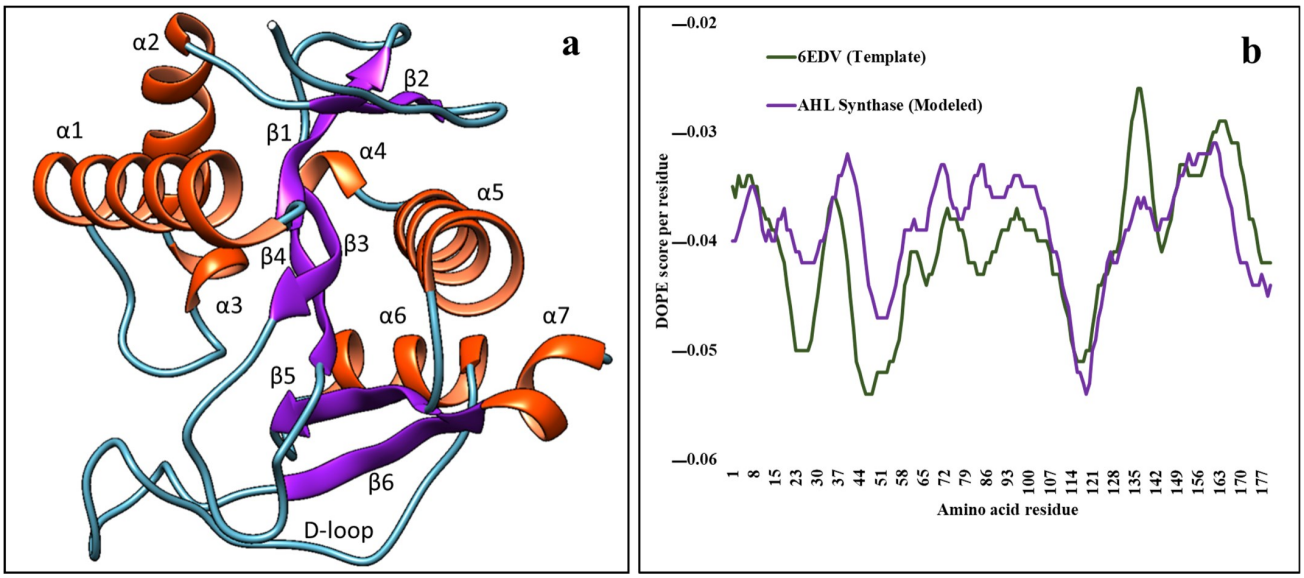


**Figure 3.** Modeled structure and DOPE profile of AHL synthase. (**a**) Modeled structure of AHL synthase in Desulfovibrio vulgaris Hildenborough, and (**b**) DOPE profiles of modeled AHL synthase and template structure (6EDV).

### 2.3. Analysis of Modelled AHL Synthase Structure with Others Present in Protein Data Bank

Our results showed the presence of 111 different genes (e.g., lasI, traI, expI, ainS, esaI etc., Figure 2) coding for different AHL synthases in 5907 different bacteria. Two AHL synthases (EsaI and LasI) were chosen as base models to compare the structural similarity with the modeled DvH AHL synthase.

EsaI was the fifth most common AHL synthase, shared amongst 35 different bacterial genera (Figure 2). EsaI produces AHL molecules with intermediate length (3-oxo-C6-HSL) and, to a lesser extent, also produces 3-oxo-C8-HSL and 3-oxo-C12-HSL. The EsaI structure (PDB ID #1KZF) of Pantoea stewartii was determined by Watson and Minogue using X-ray diffraction at a resolution of 1.80 Å [46]. The refined EsaI structure consists of a mixed -fold consisting of a cleft and two well-defined cavities for catalysis [46]. The V-shaped active site is shaped by eight-stranded sheet surrounded by nine -helices. The N-terminus consists of hydrophobic or charged conserved residues and has the least sequence variability. The substrate (acyl carrier protein, acpP) carrying the acyl group interacts with this hydrophobic region in EsaI [28,52]. The T140 residue in the active site catalyzes the production of AHL molecules with -oxo or -OH group; however, the replacement of T140 by either glycine or alanine in AHL synthases such as RhlI, CerI, AsaI, and SwrI produces AHL without -oxo or -OH group. Other AHL synthases (LuxS, AinS, VanM) in different gram-negative bacteria share sequence homology with the conserved block 3 region in EsaI [28,52].

LasI was the most common AHL synthase, shared between 120 different bacterial genera (Figure 2). LasI synthesizes AHL molecules with longer chain (3-oxo-C12-HSL)

than those produced by other AHL synthases [53]. LasI structure (PDB ID #1RO5) of Pseudomonas aeruginosa has been determined by Gould and Schweizer using X-ray diffraction at a resolution of 2.3 Å [54]. The overall structure of LasI consists of an alternate () sandwich containing eight -helices surrounded by nine -strands. The active site is a V-shaped cleft (V-cleft) between two parallel -strands (4 and 5) [54]. There is also the presence of -bulge in the 4 beta-strands. This -bulge was observed in EsaI AHL synthase, and it is conserved amongst all members of AHL synthase family [46,54]. The N-terminal half of LasI adjacent to V-cleft consists of a large electrostatic cluster of highly conserved residues in the AHL-synthase family. Additionally, water molecule bound to Glu101 residue in LasI is also conserved in other AHL-synthases and is involved in the cat-alytic mechanism of the AHL-synthases. Another important feature of all AHL synthases is the acyl chain binding site in the active center of the enzyme. The acyl-chain binding site in LasI is a hydrophobic tunnel that is specific to the C12 acyl group. Specific residues, such as Met79, Phe105, Thr142 and Thr144, are conserved among other AHL-synthases, and appear to position the acyl-chain in the proper orientation for subsequent catalysis. The different size of the hydrophobic side chains in the acyl chain binding tunnel pocket determines the length of the acyl chain (C4-C18) it can accommodate. This information from both EsaI and LasI is vital in the prediction of AHL synthases in different gram-negative bacteria, including DvH.

The four PDB structures, PDB#1RO5, PDB#2P2F, PDB#6WNS, and PDB#1KZF, were superimposed with the modeled structure using PYMOL align command to compare the structural properties between the different AHL synthases responsible for the synthesis of different types of AHL molecules. Root mean square deviation (RMSD, Å) between the molecules showed a significant deviation at the central carbon atoms of the beta turns between the AHL synthases downloaded from PDB and the modeled AHL synthase (model:1RO5 = 2.037; model:3P2F = 1.270; model:6WNS =1.381; model:1KZF= 1.78). The superimposition between the modeled AHL synthase and the selected AHL synthases are shown in Figure S4. The properties of the modeled AHL synthase in terms of -helices and sheets arrangement were compared to the above structures and are represented in the form of presence-absence matrix in Table 1. The modeled AHL synthase structure consists of seven right-handed -helices and six sheets (three pairs of anti-parallel sheets, Figure 3). In contrast to the PDB structures of AHL synthases, two smaller helices (3 and 4) were observed at the N- and C-terminus of the protein (Figure 3); however, no significant role was noticed during interactions or folding. The D-loop was observed near the catalytic center, the charged amino acid of which contributes to the passaging of substrates through the tunnels.

**Table 1.** The presence-absence matrix of the -helices and sheets compared between the modeled AHL and the known AHL synthases.

| Fold Type | Modeled AHL | IRO5 (LasI) | 2P2F | 6WNS | IKZF (EsaI) |
|---|---|---|---|---|---|
| 1 RH 2 | X | X | X | X | X |
| RH 3 | X | X | X | X | X |
| RH 4 | X | X | X | X | X |
| RH 5 | X | X | X | X | X |
| RH 6 | X | X | X | X | X |
| RH 7 | X | X | X | X | X |
| RH | X | X | X | X | X |
| 1 AP(2) 2 | X | X | X | X | X |
| AP(1) 3 | X | X | X | X | X |
| AP(4) 4 | X | X | X | X | X |
| AP(3) 5 | X | X | X | X | X |
| AP(6) 6 | X | X | X | X | X |
| AP(5) | X | X | X | X | X |

RH: Right-handed helix; AP: Anti-parallel.

When the modeled AHL synthase was compared with the PDB# 1RO5, it was observed that, in the PDB structure of the latter, 2, 3, and 4 were missing (Table 1). In the modeled AHL synthase, 2 comprises of 18 amino acid residues (Arg43-Gln60) but did not participate in the interactions. The small helices of four and three amino acids in 3 (Pro31-Met34) and 4 (Arg101-Tyr103), respectively, were observed only in PDB# 6WNS, but 3 is also present in PDB# 1KZF. 7 (His176-Arg181), which comprises of six residues, is missing only in PDB# 2P2F and PDB# 6WNS (Table 1); however, none of these residues were observed to have interactions with any poses of the AHL substrates. The modeled AHL synthase contained six sheets, but IKZF did not have 2 and 4 sheets (Table 1).

### 2.4. Interaction between AHL Synthase and ACP Bound Fatty Acyl Chain

AHL synthase catalyzes the transfer of fatty acyl group attached to ACP to S-adenosyl-L-methionine (SAM) [54]. In this reaction, AHL synthases utilizes SAM as amino donor and acylated ACP as the acyl chain donor [55]. AHL synthases then undergoes acylation and lactonization to generate specific AHL molecules of varying carbon chain length. The internal lactonization of SAM involves specific conformational changes in AHL synthase. However, SAM is a conserved substrate for all AHL synthases, and synthesis of AHL molecules is solely determined by the carbon chain length of acyl group in acylated-ACP [32,46]. Site-specific mutational studies have identified certain amino acid residues in the active site of AHL synthases that play a crucial role in the catalytic reactions that result in the formation of AHL molecules of different carbon chain length [56].

One important parameter that impacts synthesis of different carbon chain AHL molecules is the acyl chain length tolerance of different types of AHL synthases [57]. For example, in the study by Dong and Frane [57], catalytic efficiency of BjaI AHL synthase was remarkably reduced with increasing acyl chain length, and no synthase activity could be detected using acyl chains of length C8 or longer. In contrast, AHL synthases, such as LasI and TofI, can synthesize longer chain AHL molecules, such as 3-oxo-C12-HSL and C8-HSL [54,58]. Comparative structural analysis of acyl chain-binding cavity shows that many amino acid residues that line the hydrophobic cavity share largely conserved or are substituted with similar residues in all AHL synthases [57]. For example, in case of BjaI, amino acid residues, such as Tyr104 (Phe in LasI, EsaI and TofI), Met139 (Thr in LasI, and TofI, and Val in EsaI), and Trp143 (Met in EsaI and TofI, Val in LasI), are present in the hydrophobic binding cavity. The hydrophobic residues actively involved in the binding of acyl chain in DvH were Leu99, Trp104, Arg139, Trp97, and Tyr36. However, the specificity towards acyl chain length is determined by the highly divergent residues at the top of the active site pocket (also known as tunnel). These divergent residues result in tunnels that vary considerably in volume. For instance, Trp101/Phe147 pair that encapsulates the tunnel pocket in BjaI results in a binding cavity that only accommodates C8 acyl chain substrate. On the contrary, Leu102/Met152 at the tunnel pocket in LasI can accommodate C12 acyl chain substrate. The residues in the tunnel cavity of DvH AHL synthase identified in this study consist of Phe37, Trp97, Phe132, Ser140, His169, Tyr36, Ala134, Leu166, and Pro165 and showed the hydrophobicity and polarity of the lining sidechains as 0.16 and 8.84, respectively. The layer-weighted analysis of the physiochemical properties of lining sidechains showed the hydropathy, hydrophobicity, and polarity as 0.45, 0.03, and 7.29, respectively.

The interaction of AHL synthase with different carbon length (C4–C18) was analyzed in this study by performing docking between the modeled AHL synthase structure and the individual acyl chain substrates with different carbon chain length. The binding energies of interaction were determined by virtual screening technique using PyRx v0.8. The binding energy between the predicted AHL synthase and different acyl chain ligands obtained from literature is shown in Figure 4a. The highest (most negative) binding energy amongst all the substrates was observed in C4-acyl chain when docked with AHL synthase ( 7.2 kcal/mol). The binding energy for C6 acyl chain was 7 kcal/mol and binding energies for C8, C10, and C12 acyl chain was 7.1 kcal/mol. Interestingly, acyl chains modified with -Oxo or

-OH group had low binding energies (Figure 4a), implying the inability of AHL synthase to effectively bind these modified acyl chains. The inability of AHL synthase to bind modified acyl could also be due to the fact that the pocket sites (PS) (binding sites) for the molecules with different physical dimensions are different, and the binding site cavity tunnel's diameter is unable to accommodate modified acyl chains. The binding sites of acyl chain substrates are marked as PS, as depicted in Figure 4b. Pocket site 1 (PS1) shows the interaction of acyl chain substrates (C4, C6, C8, C10, C12), wherein the substrates are graved within the V-shaped active site cavity formed between two anti-parallel sheets (3 and 4). The formation of a characteristic -bulge in the 4 beta-strand was also observed in EsaI AHL synthase, and it is conserved amongst all members of AHL synthase family [46,54]. Leu99, Trp104, Arg139 Trp97, and Tyr36 were the interacting residues at the PS1 and are shown in Figure 5. Figure 5a–e shows the interactions between the modeled AHL synthase and the substrates (C4 to C12). The details of each interaction between the modeled AHL and the AHL precursor substrates are listed in Table S4.

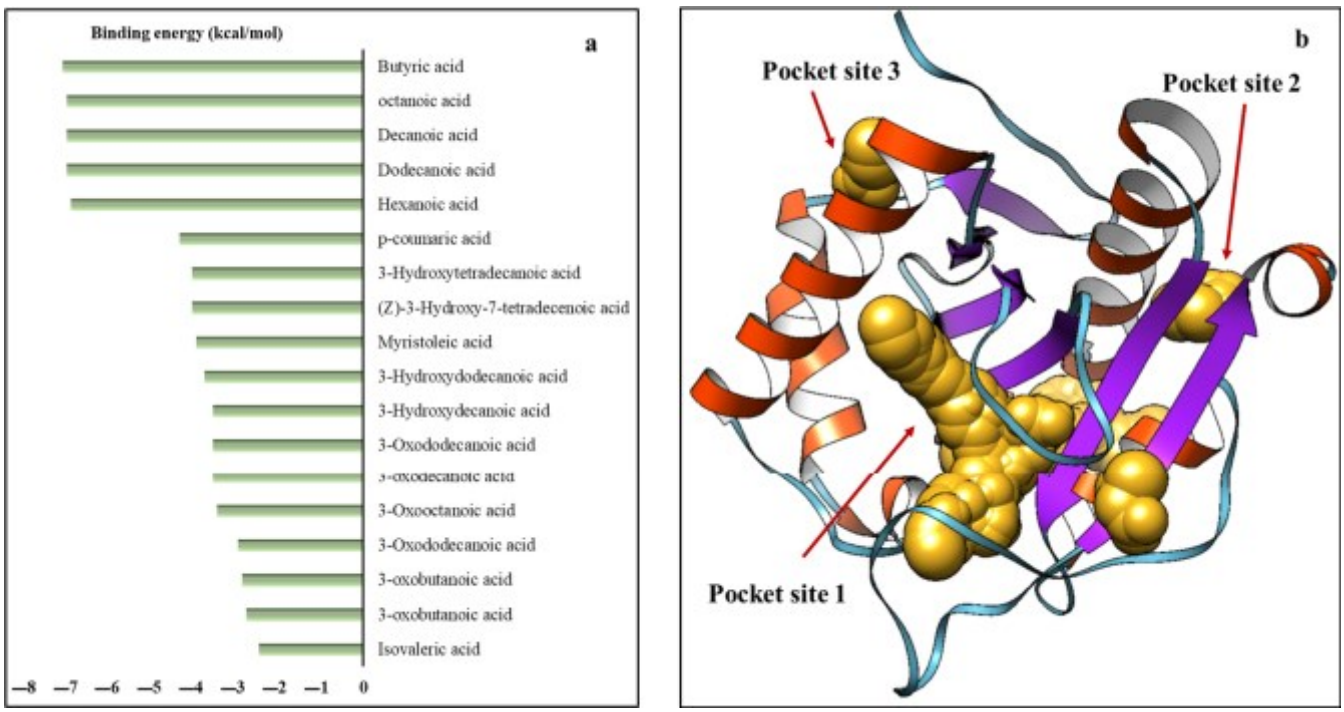


**Figure 4.** Binding energy and surface interactions between substrates and modeled AHL synthase. (**a**) Plot of binding energies between substrates and modeled AHL synthase, and (**b**) the surface interactions between the acyl substrate and modeled AHL synthase. The acyl chain substrate is shown as golden spheres.

We observed that Leu99, Trp104, and Arg139 are the interacting residues that are present consistently during the docking of modeled AHL synthase and the unsubstituted AHL precursor substrates (C4-AHL to C12-AHL). Leu99 was found to interact with the C4-AHL precursor with an alkyl hydrophobic bond with length 4.08 Å. However, in the rest of the precursors (C6-AHL to C12-AHL), polar H-N group from the Leu99 (as H-donor) formed a conventional hydrogen bond of average distance 2.9 Å with the nucleophilic center (double bonded oxygen in the fatty acid chain) of the substrates (as H-acceptor). The Pi-orbitals of Trp104 formed hydrophobic Pi-alkyl bonds (average length 4.8 Å with the substrates due to inductive effect from the carboxylic acid) on the carbons at the hydrophilic polar head of fatty acid chain. The Arg139 formed a conventional hydrogen bond (average length of 2.6 Å) with hydrogen as the donor from the protein side chain and oxygen as the acceptor from the non-polar hydrophobic tail of the acyl substrates. In case of C6-AHL precursor, Arg139 was observed to form an alkyl bond of 5.09 Å with

the substrate. Interestingly, an additional Pi-alkyl bond (5.31 Å) was present between the C6-AHL precursor and the Tyr36. Another case of alkyl bond (3.68 Å) formation was observed during the molecular docking analysis of C4-AHL precursor. More remarkably, in the case of C12-AHL precursor (shown in Figure 5e), the Pi-orbitals of Trp97 formed four additional Pi-alkyl bonds each of length: 4.21, 3.83, 5.27.and 4.18 Å, respectively. Furthermore, these results can be explained using the hydrophobicity analyses of the pockets, as discussed below.

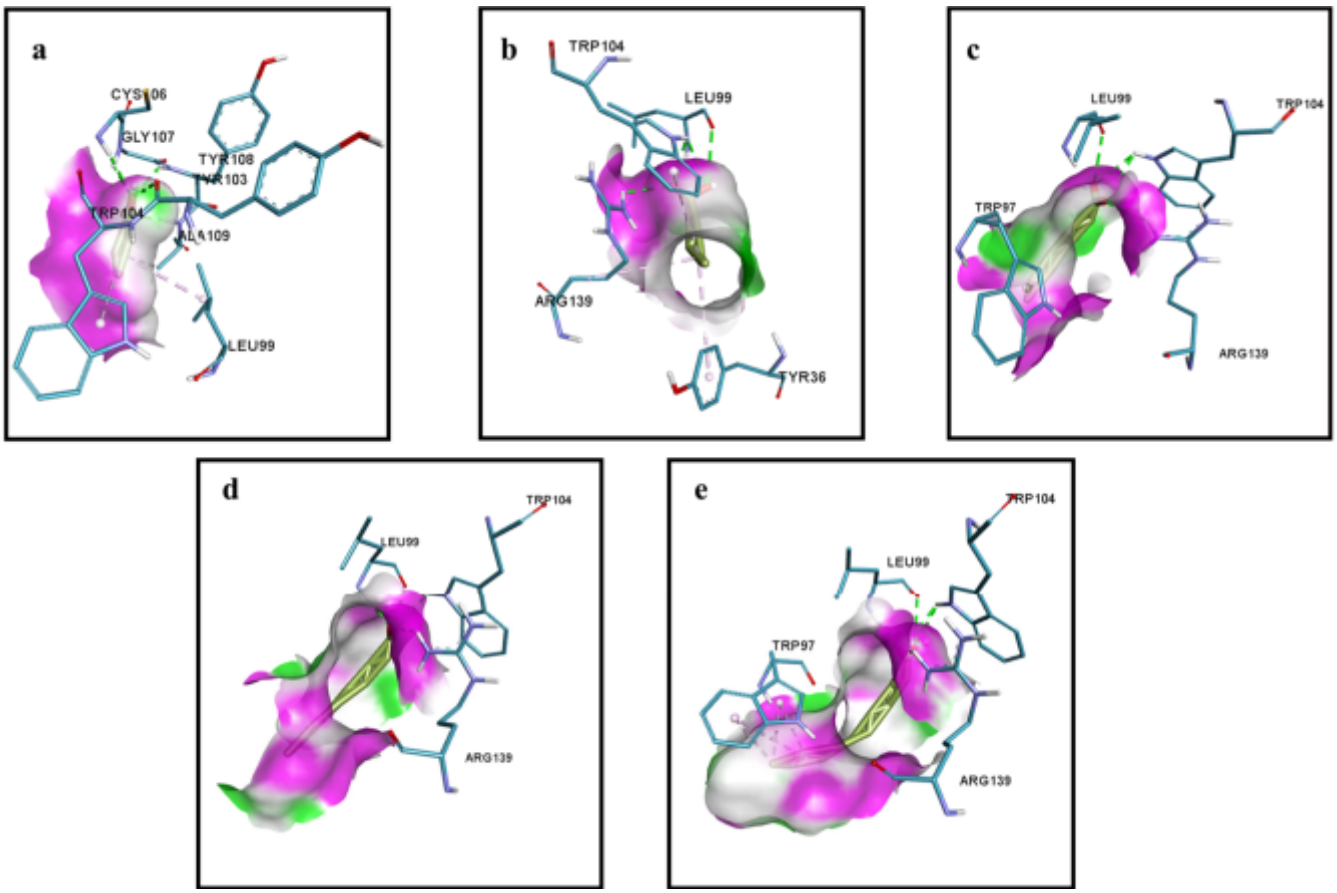


**Figure 5.** The docking interactions between the AHL synthase and unsubstituted AHLS. (**a**) C4-AHL, (**b**) C6-AHL, (**c**) C8-AHL, (**d**) C10-AHL, and (**e**) C12-AHL.

We found that the 4 (Thr93-Leu99), which consists of Leu99, one of the crucial interacting residues, is present in PDB# 1RO5 and 2P2F but not in 6WNS and 1KZF (Table 1). In addition, the interacting residue Trp97, which is only present during the binding of C8-AHL precursor, also lies on the 4. Trp104 was observed within the D-loop of the modeled AHL synthase that connects the 6 with 3, which was observed during the superimposition but, as mentioned, 3 was absent in PDB# 1RO5 and 2P2F. Arg139, which falls within the 1 (Thr138-Leu147), is conserved in all the compared AHL synthases in our study. Besides, Tyr36, which was observed to be one of the interacting residues only in C6-AHL precursor, is present within the loop that connects 2 and 4, and is notably present in all the AHL synthases, despite of the absence of 2 and 4 in a few synthases. Therefore, the D-loop, -helices and -sheets that comprise the interacting amino acid residues from the-modeled AHL synthase are also found in the existing AHL synthases.

The three hydrophobic pockets and tunnels picturized using the hydrophobic surface display in Chimera v1.14 are shown in Figure 6a. The 5-Residue Moving Average Hydrophobicity, analyzed using Discovery Studio v20, is shown in Figure 6d. The hydrophobicity index, determined using the Kyle and Doolittle algorithm, showed positive numbers for hydrophobic residues that govern the active sites. Hydrophobicity analysis

showed the possibility of three cavities and seven tunnels in the putative AHL synthase with a minimum bottleneck radius set to 1.25 Å, as shown in Figure 6b. The longest tunnels among these three cavities were found in the cavity of PS1, with each of lengths 15.36, 15.50, and 16.57 Å, and average volume of 2811 Å$^3$, while the average length and volume of the cavities from PS2 and PS3 are 7.50 Å$^3$ and 402 Å$^3$, respectively. Figure 6c shows the variation of free radius and actual radius of the tunnel (with length 15.36 Å) with the distance from the cavity pore. This tunnel is responsible for the diffusion of substrates into the cavity pore, as suggested from the values of actual radius, which are large enough for the penetration of larger fatty acid chains. The different volumetric values of the cavities suggest that 1 and 2-helices, and 3 and 4 sheets are equally important for the diffusional travel of molecules through the membrane and regulate the penetration of molecules to the active site.

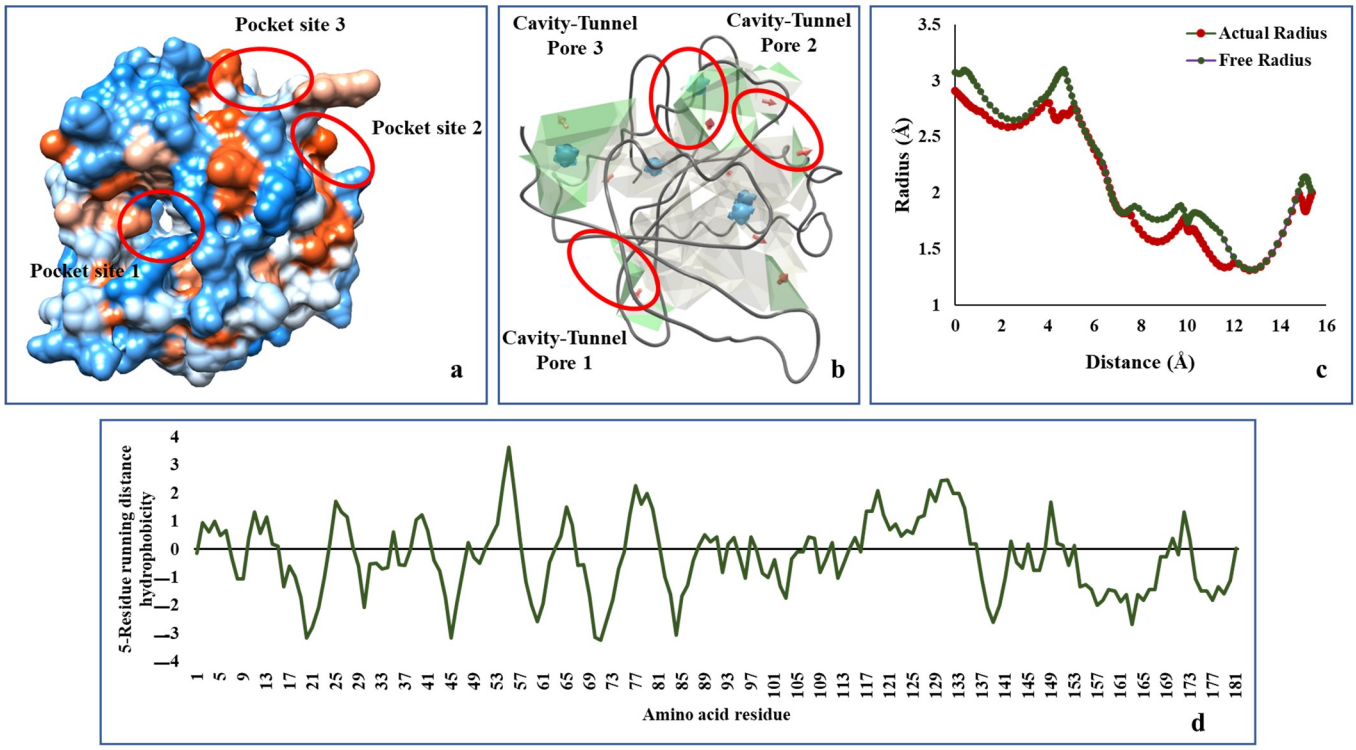


**Figure 6.** (**a**) The solvent accessible and nonpolar hydrophobic cavities in solid surface display, (**b**) the hydrophobic tunnels and cavities, (**c**) the variation of radius with the distance from the tunnel pore, and (**d**) 5-Residue Moving Average Hydrophobicity of AHL synthase.

The comparative binding energy values between acyl chains suggested that the higher the depth of the cavity and the greater the length of the tunnel, the more the binding energy. The tunnel distance to radius variations for PS2 and PS3 are shown in Figure S5a,b, respectively. The tunnel pore radius for PS2 and PS3 are 1.4, and 1.5 Å, respectively, and are not enough for the diffusional penetration of the substrates. Additionally, in the docking studies, it was observed that only a few (<3) substrates can be allowed within the PS1 and PS2 but with different orientation, and higher structural variations. Thus, in conclusion, PS1 is highly specific to the geometry of the substrate, and there is presence of only one active site within the modeled AHL synthase.

The interaction study between the modeled AHL synthase and acyl chain substrates revealed the presence of hydrophobic nonpolar and charged amino acids that interacted at the active site. When acyl chains were docked with the modeled AHL synthase, the interacting residues in the PS1 were Leu99, Trp104, Arg139, Trp97, and Tyr36. According to the hydrophobicity index of the amino acid residues surrounding the pocket sites, the residues are nonpolar and hydrophobic, which contributed to the non-electrostatic bonds

between the residues and the substrates. The electrostatic and non-electrostatic bonds together formed an intact enzyme-substrate complex. The binding energies between the substrates and pocket sites are considerably too low to participate in allosteric inhibition. The binding energy approach and hydrophobicity approach data suggest that PS1 is the active site in AHL synthase.

## 3. Materials and Methods

### 3.1. Data Mining and Multiple Sequence Alignment to Find an AHL Synthase Gene in Desulfovibrio vulgaris Hildenborough

The complete collection of acyl homoserine lactone synthase (AHL) genes and corresponding protein sequences were retrieved from UniProtKB. "Acyl homoserine lactone synthase" was searched as a query in the UniProt knowledgebase (UniProtKB) [59], and all AHL synthases (including both experimental and computationally annotated) were selected based on their gene ontology terms (molecular function (MF) and biological process (BP)). All the proteins selected had MF and BP assigned as N-acyl homoserine lactone synthase activity and quorum sensing, respectively. The amino acid sequences of all the AHL synthases downloaded from UniProt were further sorted based on gene names using a custom python script to remove duplicated proteins. A total of 111 different genes coding for different AHL synthases from 5907 different bacteria were found.

Multiple sequence alignment (MSA) using NCBI standalone BLAST was performed to align all the AHL synthases (amino acid sequences) for conserved domain analysis. The consensus sequence identified was then validated using InterPro Scan and Pfam databases [60,61]. European Molecular Biology Open Software Suite (EMBOSS) Backtranseq was used to reverse-translate the amino acid consensus sequence to nucleotide sequence [62]. MSA was then used to align the reverse-translated consensus sequence (nucleotides) to the DvH genome sequence (nucleotides). The open reading frame (ORF) aligned region in DvH genome was established using ORF finder tool in NCBI. The workflow summarizing the steps of consensus sequence-based ORF identification is depicted in Step 1 of Figure 7.

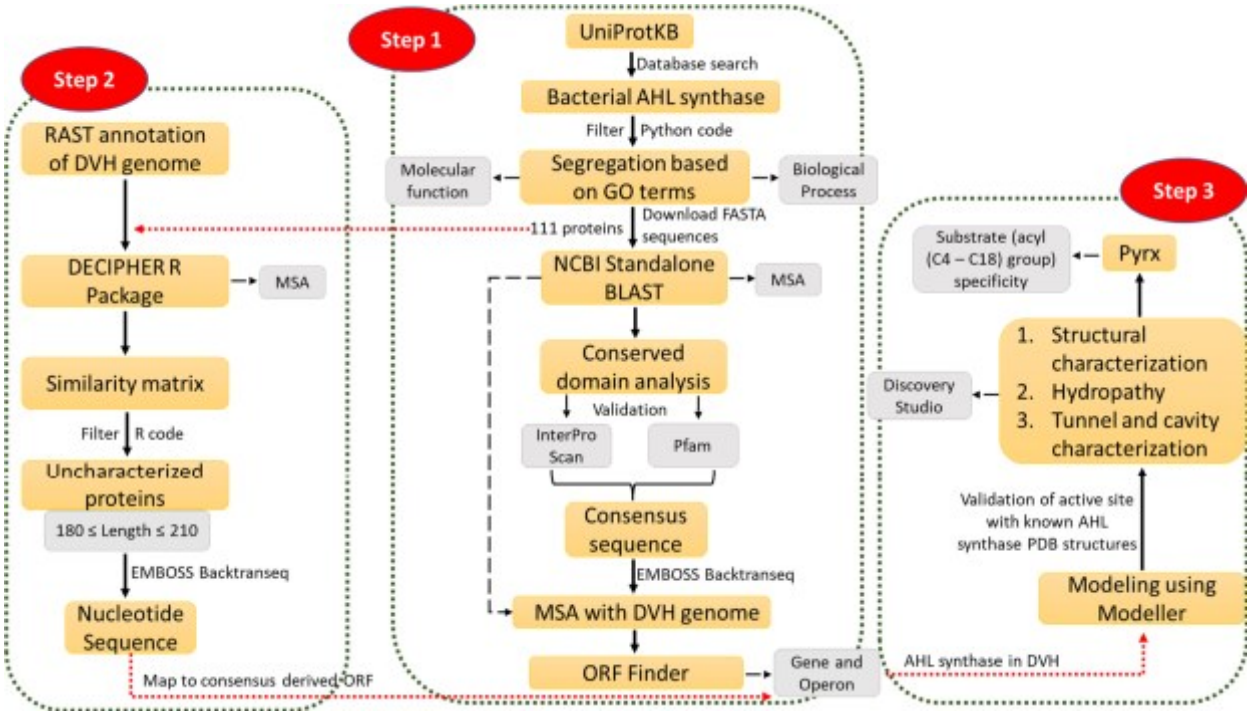


**Figure 7.** Workflow for the identification and homology modeling of AHL synthase in DvH.

To annotate the above identified ORF, the two contigs of DvH (taxonomy ID 882) were downloaded from NCBI website (Accession No. CABHLV010000001.1 and CABHLV010000002.1). These contigs were annotated using rapid annotation using subsystem technology (RAST v2.0) online software [63], and the annotated genome protein sequences were downloaded. MSA with the amino acid sequences was performed between the 111 AHL synthases sorted in Step 1 and all the proteins (annotated and uncharacterized) from DvH using the DECIPHER package in R programming language [64]. DECIPHER resulted in the formation of similarity matrix between the sorted and DvH genes. All the uncharacterized proteins in DvH were then filtered based on amino acid sequence length between 170 and 225. This sequence length was chosen since all the monomeric AHL synthase mined from UniProtKB were between 170 to 225 amino acids in length. This resulted in a manageable uncharac-terized protein set satisfying the criteria of protein sequence length as well as identity of >20% [24]. This protein set was then reverse translated to their corresponding nucleotide sequences (confined to bacterial genetic code of Escherichia coli to avoid codon biasness) and aligned to the consensus sequence derived in Step 1 (Figure 7). The steps involving annotation of DvH genome and mapping of consensus sequence to uncharacterized genes are shown in Figure 7 (Step 2). The most probable AHL synthase in DvH that has the same motif as in the 111 AHL synthase genes was obtained. The gene ID for this uncharacterized protein was DVU_2486, and its UniProt Id was Q728W6.

### 3.2. Modelling of AHL Synthase in Desulfovibrio vulgaris Hildenborough

The modeling of AHL synthase structure (Q728W6) was performed using the homology modeling technique using Modeler v10.2 [65]. The amino acid FASTA sequence of the AHL synthase of DvH was retrieved from the UNIPROT database. The pdball.pir.gz file containing sequences for all PDB structures was downloaded from modeler website (https://salilab.org/modeller/supplemental.html (accessed on 26 February 2022)). The PDB structures downloaded were compared against the query protein AHL synthase, to determine the homology percentages. NCBI-BLASTP was also performed using BLOSUM62 substitution matrix and protein-specific iteration (PSI) algorithm to confirm and validate the best homology template, with good query coverage [66]. The best PDB structure for AHL synthase of DvH were used as a single template to model the protein. The best model was selected out of 20 predicted models with the help of discrete optimized protein energy (DOPE) score and GA341 score.

For the AHL synthase of DvH, the initial geometry of the best model was analyzed using Modeller v10.2 by comparing and plotting the DOPE per residue score between the template structure and the best model structure. The stereochemical properties of the modeled structure of AHL synthase were further improved using the loop refinement technique [67]. Loop refinement is used when the overall target structure deviates from the template structure due to differences in amino acid sequence. The structural aspects that originate due to these differences in sequences are optimized using an ab-initio structure refinement approach [68]. Loop refinements were performed in Chimera v1.14 using Modeller v10.2 loop optimization script with manually adjusted torsion angles. The steric hindrance was minimized, and the geometry of the protein was improved through a large set of trials with restraints, such as torsion angles, Lennard-jones potentials, CA-CB and CA-CA bonds. The range of torsion angles (Phi, ’ and Psi, ) between polypeptide chains define the flexibility of the protein backbone and its ability to adopt a specific 3D fold. Lennard–Jones potential governs the strength of interaction and repulsion between a pair of atoms in the protein structure and gives the lowest free energy at which the protein is stable. The final modeled and refined structure of AHL synthase was further subjected to energy minimization using CHARM22_PROT and CHARM22_CHAR force-field algorithm in VEGAZZ 2.0.8 and nanoscale molecular dynamics (NAMD) with 100 conjugate descent steps (step size 0.01), and dielectric constant of 4.0 [69,70]. The Ramachandran statistics for the modeled structure of AHL synthase was performed using MolProbity structure validation web service software [71]. Stereochemical superimposition of the atoms between

the template protein and target protein was validated by the root mean square deviation (RMSD) analysis using PYMOL (Schrödinger, New York, USA.).

### 3.3. Selection and Designing the Substrates of AHL Synthase

Substituted (oxo- and hydroxy-) and unsubstituted acyl classes (C4–C18) are the substrates for AHL synthase. Depending on the acyl class specificity, acyl molecules are carried by acpP to the AHL synthase, where it fuses with the homoserine lactone at the catalytic center of the enzyme to synthesize acyl homoserine lactones [13]. The candidate acyl molecules were chosen from published literature and were used as individual substrates, as shown in the supplementary information (Table S5) [23,33,72–81]. The canonical SMILES for all the substrates were downloaded from PubChem database, with CIDs listed in Table S5, and the structures were modeled using the build editing tool in Chimera v1.14; the 2D chemical structures are shown in Table S6. The energies of the intended substrates were minimized using the minimize structure option (following CHARM36 force-field algorithm) with 1000 steepest descent steps and 100 conjugate gradient steps at a size of 0.02Å. The polar hydrogen and Gasteiger–Marsih charges were added to all standard and non-standard residues to count the optimized terminal charge [82]. The individual structures in PDB format were then saved into a single PDB file using Open Babel v2.4.1 [83].

### 3.4. Interaction between the Substrates and Modelled AHL Synthase

PyRx v0.8 was used to screen the substrates by performing a docking analysis between the protein model and the set of substrates using Vina v4.2 algorithm [51,84,85]. The macromolecule (AHL synthase) and the ligand (substrate) structures were loaded in the workspace and were converted into PDBQT files. The grid box dimensions for x, y, and z coordinates were set at 40.77 Å, 48.20 Å, and 41.62 Å, respectively, so that the grid box covers the entire protein. The exhaustiveness of the system that regulates the number of independent runs, conformational flexibility of the ligands, and objective scoring function, was set to 8. There were nine binding energies for each ligand–protein interaction that were confined to nine possible conformers. The best conformer inter-action between the ligand and the substrate was selected on the basis of highest negative binding energy and minimum RMSD of the ligand.

### 3.5. Analysis of Hydropathy and Tunnels within the AHL Synthase of Desulfovibrio vulgaris Hildenborough

The hydrophobicity index of the amino acid residues of the modeled structure was analyzed using the Kyle and Doolittle algorithm in Discovery Studio (DS v20) [86]. The values of the hydrophobicity were plotted using ggplot2 package in R programming language, and the 5-Residue Moving Average Hydrophobicity curves were analyzed using the hydrophobicity chart in DSv20 to confirm the hydrophobic pockets within the modeled structure. The lengths of the tunnels and the depths of the cavities were determined using Mole v2.5.17.4.24 [87]. The interacting amino acid residues were selected, and the tunnels were evaluated by regulating the minimum bottleneck radius, pore, and length to 1.25 Å, 0 Å, and 0 Å, respectively. The cavities corresponding to each tunnel were found by setting the probe radius, and minimum depth to 8 Å, and 5 Å, respectively.

### 3.6. Superimposition between the Known and Modelled AHL Synthase

The known crystallographic structures of AHL synthases were downloaded from Protein Databank (PDB) and are listed in Table 2. The structures of AHL synthases are superimposed on to the modeled AHL synthases using Chimera v1.14 and PYMOL v1.2r3pre to infer the substrate specificity of the modeled AHL synthase and the corresponding structural characteristics of its catalytic domain.

**Table 2.** List of AHL synthases from different organisms considered during superimposition.

| AHL Synthase Gene | Organism Name | PDB ID | Resolution (Å) | Crystallography Method | References |
|---|---|---|---|---|---|
| EsaI | Escherichia coli BL21 | 1KZF | 1.80 | X-ray diffraction | [46] |
| MesI | Mesorhizobium sp. ORS 3359 | 6WNS | 1.93 | X-ray diffraction | [88] |
| LasI | Escherichia coli | 1RO5 | 2.30 | X-ray diffraction | [54] |
| TofI | Burkholderia glumae | 3P2F | 2.30 | X-ray diffraction | [58] |

## 4. Conclusions

This study used MSA, homology modeling, and docking to decode an AHL synthase gene (DVU_2486) in DvH. The operon architecture of the AHL synthase remains unstudied due to the unavailability of any known genes at the upstream and downstream regions of this operon. The motif of DVU_2486 consists of one domain that codes for AHL synthase; however, the leader sequence and the transcription nucleotide at the upstream of this gene was not detected within the identified ORF region. The next step could be to validate the function of the identified DvH AHL synthase by creating mutants e.g., AHL synthase gene knockdown or site-directed mutagenesis of crucial amino acids present in the identified active site in this study and test those for appropriate phenotypes. Finally, our approach towards the identification of AHL synthase and location of active site could be applied towards identification of other AHL synthase family members in other SRB.

**Supplementary Materials:** The following supporting information can be downloaded at: https://www.mdpi.com/article/10.3390/catal13020364/s1, Figure S1: Ramachandran plot depicting measurement of backbone dihedral angles (, phi and , psi) in acyl homoserine lactone (AHL) synthase; Figure S2: (a) The alignment of amino acids, and (b) superimposition, between the modeled AHL synthase and the template (#6EDV); Figure S3: Superimposition between the predictive AlphaFold- (green) and modeler- based (blue) structure of probable AHL synthase. Figure S4: The individual structures of (a) modeled AHL synthase, (b) PDB# 1RO5, (c) PDB# 2P2F, (d) PDB# 6WNS, and (e) PDB# 1KZF. The superimposition between the modeled AHL synthase and (f) PDB# 1RO5, (g) PDB# 2P2F, (h) PDB# 6WNS, and (i) PDB# 1KZF.; Figure S5: The actual and free radius variation with tunnel distances in (a) PS2, and (b) PS3; Table S1: A brief description of the AHL genes mentioned in Figure 2. Table S2: Stereochemical analysis of AHL synthase; Table S3: The statistical t-test between the predictive AlphaFold- and modeler- based structure of probable AHL synthase. Table S4: The detailed interactions between the modeled AHL synthase and the AHL substrates (Available as an excel file); Table S5: Details of fatty acyl molecules and their respective AHL products in different organisms reported in literature (Available as an excel file); Table S6: Candidate fatty acyl molecules and their respective chemical structures used in this study.

**Author Contributions:** Conceptualization, A.K.T. and D.S.; methodology, A.K.T. and D.S.; soft-ware, A.K.T. and D.S.; validation, P.S., P.T., S.R. and R.K.S.; formal analysis, A.K.T. and D.S.; investigation, A.K.T. and D.S.; data curation, A.K.T.; writing—original draft preparation, A.K.T.; writing—review and editing, A.K.T., P.S., P.T., S.R., D.S., K.M.G. and R.K.S.; visualization, A.K.T.; supervision, R.K.S.; project administration, R.K.S.; funding acquisition, R.K.S. All authors have read and agreed to the published version of the manuscript.

**Funding:** We gratefully acknowledge support from the National Science Foundation (Awards #1736255, #1849206, and #1920954) and the Department of Chemical and Biological Engineering at the South Dakota School of Mines and Technology. R.K.S. and K.M.G. acknowledge Universiti Teknologi Malaysia (UTM) Research Fellow grant #00P31.

**Data Availability Statement:** Not applicable.

**Acknowledgments:** We acknowledge Department of Chemical and Biological Engineering at the South Dakota School of Mines and Technology and Universiti Teknologi Malaysia (UTM).

**Conflicts of Interest:** The authors declare no conflict of interest. The funders had no role in the design of the study; in the collection, analyses, or interpretation of data; in the writing of the manuscript; or in the decision to publish the results.

## References


1. Muyzer, G.; Stams, A. The Ecology and Biotechnology of Sulphate-Reducing Bacteria. Nat. Rev. Microbiol. **2008**, 6, 441–454. [CrossRef] [PubMed]
2. Smith, M.; Bardiau, M.; Brennan, R.; Burgess, H.; Caplin, J.; Ray, S.; Urios, T. Accelerated Low Water Corrosion: The Microbial Sulfur Cycle in Microcosm. NPJ Mater. Degrad. **2019**, 3, 37. [CrossRef]
3. Ning, J.; Zheng, Y.; Brown, B.; Young, D.; Nesic, S. The Role of Pyrite in Localized H2s Corrosion of Mild Steel. In Proceedings of the CORROSION 2017, New Orleans, LA, USA, 26–30 March 2017.
4. Kato, S. Microbial Extracellular Electron Transfer and Its Relevance to Iron Corrosion. Microb. Biotechnol. **2016**, 9, 141–148. [CrossRef] [PubMed]
5. Beech, I.B.; Gaylarde, C.C. Recent Advances in the Study of Biocorrosion: An Overview. Rev. Microbiol. **1999**, 30, 117–190. [CrossRef]
6. García-Contreras, R.; Nuñez-López, L.; Jasso-Chávez, R.; Kwan, B.W.; A Belmont, J.; Rangel-Vega, A.; Maeda, T.; Wood, T.K. Quorum Sensing Enhancement of the Stress Response Promotes Resistance to Quorum Quenching and Prevents Social Cheating. ISME J. **2015**, 9, 115–125. [CrossRef]
7. Rutherford, S.T.; Bassler, B.L. Bacterial Quorum Sensing: Its Role in Virulence and Possibilities for Its Control. Cold Spring Harb. Perspect. Med. **2012**, 2, a012427. [CrossRef] [PubMed]
8. Solano, C.; Echeverz, M.; Lasa, I. Biofilm Dispersion and Quorum Sensing. Curr. Opin. Microbiol. **2014**, 18, 96–104. [CrossRef] [PubMed]
9. Verbeke, F.; De Craemer, S.; Debunne, N.; Janssens, Y.; Wynendaele, E.; Van de Wiele, C.; De Spiegeleer, B. Peptides as Quorum Sensing Molecules: Measurement Techniques and Obtained Levels in Vitro and in Vivo. Front. Neurosci. **2017**, 11, 183. [CrossRef]
10. Kawaguchi, T.; Chen, Y.P.; Norman, R.S.; Decho, A.W. Rapid Screening of Quorum-Sensing Signal N-Acyl Homoserine Lactones by an in Vitro Cell-Free Assay. Appl. Environ. Microbiol. **2008**, 74, 3667–3671. [CrossRef]
11. Scarascia, G.; Wang, T.; Hong, P.-Y. Quorum Sensing and the Use of Quorum Quenchers as Natural Biocides to Inhibit Sulfate-Reducing Bacteria. Antibiotics **2016**, 5, 39. [CrossRef]
12. Decho, A.W.; Norman, R.S.; Visscher, P.T. Quorum Sensing in Natural Environments: Emerging Views from Microbial Mats. Trends Microbiol. **2010**, 18, 73–80. [CrossRef]
13. Decho, A.W.; Visscher, P.T.; Ferry, J.; Kawaguchi, T.; He, L.; Przekop, K.M.; Norman, R.S.; Reid, R.P. Autoinducers Extracted from Microbial Mats Reveal a Surprising Diversity of N-Acylhomoserine Lactones (Ahls) and Abundance Changes That May Relate to Diel Ph. Environ. Microbiol. **2009**, 11, 409–420. [CrossRef]
14. Smith, J.L.; Fratamico, P.M.; Gunther, N.W., IV. Shiga Toxin-Producing Escherichia Coli. Adv. Appl. Microbiol. **2014**, 86, 145–197.
15. van Keulen, G.; Dyson, P.J. Production of Specialized Metabolites by Streptomyces Coelicolor A3 (2). Adv. Appl. Microbiol. **2014**, 89, 217–266.
16. Dirix, G.; Monsieurs, P.; Dombrecht, B.; Daniels, R.; Marchal, K.; Vanderleyden, J.; Michiels, J. Peptide Signal Molecules and Bacteriocins in Gram-Negative Bacteria: A Genome-Wide in Silico Screening for Peptides Containing a Double-Glycine Leader Sequence and Their Cognate Transporters. Peptides **2004**, 25, 1425–1440. [CrossRef] [PubMed]
17. Whitehead, N.A.; Barnard, A.M.; Slater, H.; Simpson, N.J.; Salmond, G.P. Quorum-Sensing in Gram-Negative Bacteria. FEMS Microbiol. Rev. **2001**, 25, 365–404. [CrossRef] [PubMed]
18. Tripathi, A.K.; Thakur, P.; Saxena, P.; Rauniyar, S.; Gopalakrishnan, V.; Singh, R.N.; Gadhamshetty, V.; Gnimpieba, E.Z.; Jasthi, B.K.; Sani, R.K. Gene Sets and Mechanisms of Sulfate-Reducing Bacteria Biofilm Formation and Quorum Sensing with Impact on Corrosion. Front. Microbiol. **2021**, 12, 3120. [CrossRef] [PubMed]
19. Vance, R.E.; Zhu, J.; Mekalanos, J.J. A Constitutively Active Variant of the Quorum-Sensing Regulator Luxo Affects Protease Production and Biofilm Formation in Vibrio Cholerae. Infect. Immun. **2003**, 71, 2571–2576. [CrossRef] [PubMed]
20. Lenz, D.H.; Mok, K.C.; Lilley, B.N.; Kulkarni, R.V.; Wingreen, N.S.; Bassler, B.L. The Small Rna Chaperone Hfq and Multiple Small Rnas Control Quorum Sensing in Vibrio Harveyi and Vibrio Cholerae. Cell **2004**, 118, 69–82. [CrossRef]
21. Park, S.; Prévost, K.; Heideman, E.M.; Carrier, M.-C.; Azam, M.S.; A Reyer, M.; Liu, W.; Massé, E.; Fei, J. Dynamic Interactions between the Rna Chaperone Hfq, Small Regulatory Rnas, and Mrnas in Live Bacterial Cells. eLife **2021**, 10, e64207. [CrossRef]
22. Lorenz, N.; Shin, J.Y.; Jung, K. Activity, Abundance, and Localization of Quorum Sensing Receptors in Vibrio Harveyi. Front. Microbiol. **2017**, 8, 634. [CrossRef]
23. Li, Z.; Nair, S.K. Quorum Sensing: How Bacteria Can Coordinate Activity and Synchronize Their Response to External Signals? Protein Sci. **2012**, 21, 1403–1417. [CrossRef] [PubMed]
24. Churchill, M.E.A.; Chen, L. Structural Basis of Acyl-Homoserine Lactone-Dependent Signaling. Chem. Rev. **2011**, 111, 68–85. [CrossRef] [PubMed]
25. Passador, L.; Cook, J.M.; Gambello, M.J.; Rust, L.; Iglewski, B.H. Expression of Pseudomonas Aeruginosa Virulence Genes Requires Cell-to-Cell Communication. Science **1993**, 260, 1127–1130. [CrossRef] [PubMed]
26. Hwang, I.; Li, P.-L.; Zhang, L.; Piper, K.R.; Cook, D.M.; Tate, M.E.; Farrand, S.K. Trai, a Luxi Homologue, Is Responsible for Production of Conjugation Factor, the Ti Plasmid N-Acylhomoserine Lactone Autoinducer. Proc. Natl. Acad. Sci. USA **1994**, 91, 4639–4643. [CrossRef]
27. Minna, P.; Flego, D.; Heikinheimo, R.; Palva, E.T. A Small Diffusible Signal Molecule Is Responsible for the Global Control of Virulence and Exoenzyme Production in the Plant Pathogen Erwinia Carotovora. EMBO J. **1993**, 12, 2467–2476.

28. Hanzelka, B.L.; Parsek, M.R.; Val, D.L.; Dunlap, P.V.; John, E.C.; Greenberg, E.P. Acylhomoserine Lactone Synthase Activity of the Vibrio Fischeri Ains Protein. J. Bacteriol. **1999**, 181, 5766–5770. [CrossRef] [PubMed]
29. Beck von Bodman, S.U.S.A.N.N.; Farrand, S.K. Capsular Polysaccharide Biosynthesis and Pathogenicity in Erwinia Stewartii Require Induction by an N-Acylhomoserine Lactone Autoinducer. J. Bacteriol. **1995**, 177, 5000–5008. [CrossRef] [PubMed]
30. Knight, T.F.; Papadakis, N.; Vibrio Fischeri Lux Operon Sali Digest. GENBANK AF170104 (Strain MJ-1); 1999. Available online: http://www.ncbi.nlm.nih.gov/nuccore/5726577 (accessed on 29 November 2022).
31. Flavier, A.B.; Ganova-Raeva, L.M.; Schell, M.A.; Denny, T.P. Hierarchical Autoinduction in Ralstonia Solanacearum: Control of Acyl-Homoserine Lactone Production by a Novel Autoregulatory System Responsive to 3-Hydroxypalmitic Acid Methyl Ester. J. Bacteriol. **1997**, 179, 7089–7097. [CrossRef]
32. Christensen, Q.H.; Brecht, R.M.; Dudekula, D.; Greenberg, E.P.; Nagarajan, R. Evolution of Acyl-Substrate Recognition by a Family of Acyl-Homoserine Lactone Synthases. PLoS ONE **2014**, 9, e112464. [CrossRef]
33. Lindemann, A.; Pessi, G.; Schaefer, A.L.; Mattmann, M.E.; Christensen, Q.H.; Kessler, A.; Hennecke, H.; Blackwell, H.E.; Greenberg, E.P.; Harwood, C.S. Isovaleryl-Homoserine Lactone, an Unusual Branched-Chain Quorum-Sensing Signal from the Soybean Symbiont Bradyrhizobium Japonicum. Proc. Natl. Acad. Sci. USA **2011**, 108, 16765–16770. [CrossRef] [PubMed]
34. Gotschlich, A.; Huber, B.; Geisenberger, O.; Tögl, A.; Steidle, A.; Riedel, K.; Hill, P.; Tümmler, B.; Vandamme, P.; Middleton, B. Synthesis of Multiple N-Acylhomoserine Lactones Is Wide-Spread among the Members of the Burkholderia Cepacia Complex. Syst. Appl. Microbiol. **2001**, 24, 1–14. [CrossRef]
35. Cheng, F.; Ma, A.; Zhuang, G.; Fray, R.G. Exogenous N-Acyl-Homoserine Lactones Enhance the Expression of Flagella of Pseudomonas Syringae and Activate Defence Responses in Plants. Mol. Plant Pathol. **2018**, 19, 104–115. [CrossRef] [PubMed]
36. Ochsner, U.A.; Reiser, J. Autoinducer-Mediated Regulation of Rhamnolipid Biosurfactant Synthesis in Pseudomonas Aeruginosa. Proc. Natl. Acad. Sci. USA **1995**, 92, 6424–6428. [CrossRef] [PubMed]
37. Oh, M.H.; Choi, C.H. Role of Luxir Homologue Anoir in Acinetobacter Nosocomialis and the Effect of Virstatin on the Expression of Anor Gene. J. Microbiol. Biotechnol. **2015**, 25, 1390–1400. [CrossRef] [PubMed]
38. Chalupowicz, L.; Manulis-Sasson, S.; Itkin, M.; Sacher, A.; Sessa, G.; Barash, I. Quorum-Sensing System Affects Gall Development Incited by Pantoea Agglomerans Pv. Gypsophilae. Mol. Plant Microbe Interact. **2008**, 21, 1094–1105. [CrossRef]
39. Bassler, B.L.; Wright, M.; Showalter, R.E.; Silverman, M.R. Intercellular Signalling in Vibrio Harveyi: Sequence and Function of Genes Regulating Expression of Luminescence. Mol. Microbiol. **1993**, 9, 773–786. [CrossRef]
40. Throup, J.P.; Camara, M.; Briggs, G.S.; Winson, M.K.; Chhabra, S.R.; Bycroft, B.W.; Williams, P.; Stewart, G.S. Characterisation of the Yeni/Yenr Locus from Yersinia Enterocolitica Mediating the Synthesis of Two N-Acylhomoserine Lactone Signal Molecules. Mol. Microbiol. **1995**, 17, 345–356. [CrossRef]
41. Rosemeyer, V.; Michiels, J.; Verreth, C.; Vanderleyden, J. Luxi-and Luxr-Homologous Genes of Rhizobium Etli Cnpaf512 Contribute to Synthesis of Autoinducer Molecules and Nodulation of Phaseolus Vulgaris. J. Bacteriol. **1998**, 180, 815–821. [CrossRef]
42. Gamage, A.M.; Shui, G.; Wenk, M.R.; Chua, K.L. N-Octanoylhomoserine Lactone Signalling Mediated by the Bpsi–Bpsr Quorum Sensing System Plays a Major Role in Biofilm Formation of Burkholderia Pseudomallei. Microbiology **2011**, 157, 1176–1186. [CrossRef]
43. Niu, C.; Clemmer, K.M.; Bonomo, R.A.; Rather, P.N. Isolation and Characterization of an Autoinducer Synthase from Acinetobacter Baumannii. J. Bacteriol. **2008**, 190, 3386–3392. [CrossRef] [PubMed]
44. Chan, Y.Y.; Bian, H.S.; Tan, T.M.C.; Mattmann, M.E.; Geske, G.D.; Igarashi, J.; Hatano, T.; Suga, H.; Blackwell, H.E.; Chua, K.L. Control of Quorum Sensing by a Burkholderia Pseudomallei Multidrug Efflux Pump. J. Bacteriol. **2007**, 189, 4320–4324. [CrossRef] [PubMed]
45. Milton, D.L.; Chalker, V.J.; Kirke, D.; Hardman, A.; Cámara, M.; Williams, P. The Luxm Homologue Vanm from Vibrio Anguillarum Directs the Synthesis of N-(3-Hydroxyhexanoyl) Homoserine Lactone and N-Hexanoylhomoserine Lactone. J. Bacteriol. **2001**, 183, 3537–3547. [CrossRef] [PubMed]
46. Watson, W.T.; Minogue, T.D.; Val, D.L.; Von Bodman, S.B.; Churchill, M.E. Structural Basis and Specificity of Acyl-Homoserine Lactone Signal Production in Bacterial Quorum Sensing. Mol. Cell **2002**, 9, 685–694. [CrossRef] [PubMed]
47. Calatrava-Morales, N.; McIntosh, M.; Soto, M.J. Regulation Mediated by N-Acyl Homoserine Lactone Quorum Sensing Signals in the Rhizobium-Legume Symbiosis. Genes **2018**, 9, 263. [CrossRef] [PubMed]
48. Malott, R.J. Quorum-Sensing in Burkolderia Cenocepacia and Burkolderia Vietnamiensis. 2007. Available online: https://library-archives.canada.ca/eng/services/services-libraries/theses/Pages/item.aspx?idNumber=436330118 (accessed on 29 November 2022).
49. Kirwan, J.P.; Gould, T.A.; Schweizer, H.P.; Bearden, S.W.; Murphy, R.C.; Churchill, M.E. Quorum-Sensing Signal Synthesis by the Yersinia Pestis Acyl-Homoserine Lactone Synthase Yspi. J. Bacteriol. **2006**, 188, 784–788. [CrossRef] [PubMed]
50. Ortori, C.A.; Atkinson, S.; Chhabra, S.R.; Cámara, M.; Williams, P.; Barrett, D.A. Comprehensive Profiling of N-Acylhomoserine Lactones Produced by Yersinia Pseudotuberculosis Using Liquid Chromatography Coupled to Hybrid Quadrupole–Linear Ion Trap Mass Spectrometry. Anal. Bioanal. Chem. **2007**, 387, 497–511. [CrossRef]
51. Samanta, D.; Govil, T.; Saxena, P.; Gadhamshetty, V.; Krumholz, L.R.; Salem, D.R.; Sani, R.K. Enhancement of Methane Catalysis Rates in Methylosinus Trichosporium Ob3b. Biomolecules **2022**, 12, 560. [CrossRef]
52. Puskas, A.; Greenberg, E.P.; Kaplan, S.; Schaefer, A.L. A Quorum-Sensing System in the Free-Living Photosynthetic Bacterium Rhodobacter Sphaeroides. J. Bacteriol. **1997**, 179, 7530–7537. [CrossRef]

53. Hoang, T.T.; Ma, Y.; Stern, R.J.; McNeil, M.R.; Schweizer, H.P. Construction and Use of Low-Copy Number T7 Expression Vectors for Purification of Problem Proteins: Purification of Mycobacterium Tuberculosis Rmld and Pseudomonas Aeruginosa Lasi and Rhli Proteins, and Functional Analysis of Purified Rhli. Gene **1999**, 237, 361–371. [CrossRef]
54. Gould, T.A.; Schweizer, H.P.; Churchill, M.E.A. Structure of the Pseudomonas Aeruginosa Acyl-Homoserinelactone Synthase Lasi. Mol. Microbiol. **2004**, 53, 1135–1146. [CrossRef] [PubMed]
55. Moré, M.I.; Finger, L.D.; Stryker, J.L.; Fuqua, C.; Eberhard, A.; Winans, S.C. Winans. Enzymatic Synthesis of a Quorum-Sensing Autoinducer through Use of Defined Substrates. Science **1996**, 272, 1655–1658. [CrossRef]
56. Shin, D.; Gorgulla, C.; Boursier, M.E.; Rexrode, N.; Brown, E.C.; Arthanari, H.; Blackwell, H.E.; Nagarajan, R. N-Acyl Homoserine Lactone Analog Modulators of the Pseudomonas Aeruginosa Rhll Quorum Sensing Signal Synthase. ACS Chem. Biol. **2019**, 14, 2305–2314.
57. Dong, S.-H.; Frane, N.D.; Christensen, Q.H.; Greenberg, E.P.; Nagarajan, R.; Nair, S.K. Molecular Basis for the Substrate Specificity of Quorum Signal Synthases. Proc. Natl. Acad. Sci. USA **2017**, 114, 9092–9097. [CrossRef] [PubMed]
58. Chung, J.; Goo, E.; Yu, S.; Choi, O.; Lee, J.; Kim, J.; Kim, H.; Igarashi, J.; Suga, H.; Moon, J.S.; et al. Small-Molecule Inhibitor Binding to an N-Acyl-Homoserine Lactone Synthase. Proc. Natl. Acad. Sci. USA **2011**, 108, 12089–12094. [CrossRef] [PubMed]
59. Uniprot: The Universal Protein Knowledgebase in 2021. Nucleic Acids Res. **2021**, 49, D480–D489. [CrossRef]
60. Quevillon, E.; Silventoinen, V.; Pillai, S.; Harte, N.; Mulder, N.; Apweiler, R.; Lopez, R. Interproscan: Protein Domains Identifier. Nucleic Acids Res. **2005**, 33, W116–W120. [CrossRef]
61. Finn, R.D.; Bateman, A.; Clements, J.; Coggill, P.; Eberhardt, R.Y.; Eddy, S.R.; Heger, A.; Hetherington, K.; Holm, L.; Mistry, J.; et al. Pfam: The Protein Families Database. Nucleic Acids Res. **2014**, 42, D222–D230. [CrossRef]
62. Rice, P.; Longden, I.; Bleasby, A. Emboss: The European Molecular Biology Open Software Suite. Trends Genet. **2000**, 16, 276–277. [CrossRef]
63. Aziz, R.K.; Bartels, D.; Best, A.A.; DeJongh, M.; Disz, T.; Edwards, R.A.; Formsma, K.; Gerdes, S.; Glass, E.M.; Kubal, M.; et al. The Rast Server: Rapid Annotations Using Subsystems Technology. BMC Genom. **2008**, 9, 1–15. [CrossRef]
64. Wright, E.S. Decipher: Harnessing Local Sequence Context to Improve Protein Multiple Sequence Alignment. BMC Bioinform. **2015**, 16, 322. [CrossRef] [PubMed]
65. Fiser, A.; Šali, A. Modeller: Generation and Refinement of Homology-Based Protein Structure Models. In Methods in Enzymology; Elsevier: Amsterdam, The Netherlands, 2003; pp. 461–491.
66. Johnson, M.; Zaretskaya, I.; Raytselis, Y.; Merezhuk, Y.; McGinnis, S.; Madden, T.L. Ncbi Blast: A Better Web Interface. Nucleic Acids Res. **2008**, 36, W5–W9. [CrossRef] [PubMed]
67. Fan, H.; Mark, A.E. Refinement of Homology-Based Protein Structures by Molecular Dynamics Simulation Techniques. Protein Sci. **2004**, 13, 211–220. [CrossRef] [PubMed]
68. Lee, G.R.; Heo, L.; Seok, C. Effective Protein Model Structure Refinement by Loop Modeling and Overall Relaxation. Proteins **2016**, 84, 293–301. [CrossRef]
69. Phillips, J.C.; Hardy, D.J.; Maia, J.D.C.; Stone, J.E.; Ribeiro, J.V.; Bernardi, R.C.; Buch, R.; Fiorin, G.; Hénin, J.; Jiang, W.; et al. Scalable Molecular Dynamics on Cpu and Gpu Architectures with Namd. J. Chem. Phys. **2020**, 153, 044130. [CrossRef]
70. Pedretti, A.; Mazzolari, A.; Gervasoni, S.; Fumagalli, L.; Vistoli, G. The Vega Suite of Programs: An Versatile Platform for Cheminformatics and Drug Design Projects. Bioinformatics **2021**, 37, 1174–1175. [CrossRef]
71. Williams, C.J.; Headd, J.J.; Moriarty, N.W.; Prisant, M.G.; Videau, L.L.; Deis, L.N.; Verma, V.; Keedy, D.A.; Hintze, B.J.; Chen, V.B.; et al. Molprobity: More and Better Reference Data for Improved All-Atom Structure Validation. Protein Sci. **2018**, 27, 293–315. [CrossRef]
72. Cooley, M.A.; Whittall, C.; Rolph, M.S. Pseudomonas Signal Molecule 3-Oxo-C12-Homoserine Lactone Interferes with Binding of Rosiglitazone to Human Ppar. Microbes Infect. **2010**, 12, 231–237. [CrossRef]
73. Parsek, M.R.; Greenberg, E.P. Acyl-Homoserine Lactone Quorum Sensing in Gram-Negative Bacteria: A Signaling Mechanism Involved in Associations with Higher Organisms. Proc. Natl. Acad. Sci. USA **2000**, 97, 8789–8793. [CrossRef]
74. Laue, B.E.; Jiang, Y.; Chhabra, S.R.; Jacob, S.; Stewart, G.S.; Hardman, A.; Downie, J.A.; O'Gara, F.; Williams, P. The Biocontrol Strain Pseudomonas Fluorescens F113 Produces the Rhizobium Small Bacteriocin, N-(3-Hydroxy-7-Cis-Tetradecenoyl) Homoserine Lactone, Via Hdts, a Putative Novel N-Acylhomoserine Lactone Synthase. Microbiology **2000**, 146, 2469–2480. [CrossRef]
75. Schaefer, A.L.; Greenberg, E.P.; Oliver, C.M.; Oda, Y.; Huang, J.J.; Bittan-Banin, G.; Peres, C.M.; Schmidt, S.; Juhaszova, K.; Sufrin, J.R. A New Class of Homoserine Lactone Quorum-Sensing Signals. Nature **2008**, 454, 595–599. [CrossRef] [PubMed]
76. Papenfort, K.; Bassler, B.L. Quorum Sensing Signal–Response Systems in Gram-Negative Bacteria. Nat. Rev. Microbiol. **2016**, 14, 576–588. [CrossRef]
77. Stock, F.; Cirri, E.; Nuwanthi, S.G.L.I.; Stock, W.; Ueberschaar, N.; Mangelinckx, S.; Pohnert, G.; Vyverman, W. Sampling, Separation, and Quantification of N-Acyl Homoserine Lactones from Marine Intertidal Sediments. Limnol. Oceanogr. Methods **2021**, 19, 145–157. [CrossRef]
78. Vajedsamiei, J.; Melzner, F.; Raatz, M.; Kiko, R.; Khosravi, M.; Pansch, C. Simultaneous Recording of Filtration and Respiration in Marine Organisms in Response to Short-Term Environmental Variability. Limnol. Oceanogr. Methods **2021**, 19, 196–209. [CrossRef]
79. Biswa, P.; Doble, M. Production of Acylated Homoserine Lactone by Gram-Positive Bacteria Isolated from Marine Water. FEMS Microbiol. Lett. **2013**, 343, 34–41. [CrossRef]

80. Kaur, J.; Yogalakshmi, K.N. Degradation of N-Hexanoyl Homoserine Lactone with Quorum Quenching Bacteria Immobilised Magnetic Nanocomposite Beads. Environ. Technol. **2022**, 43, 885–892. [CrossRef]
81. Tabraiz, S.; Shamurad, B.; Petropoulos, E.; Charlton, A.; Mohiudin, O.; Danish Khan, M.; Ekwenna, E.; Sallis, P. Diversity of Acyl Homoserine Lactone Molecules in Anaerobic Membrane Bioreactors Treating Sewage at Psychrophilic Temperatures. Membranes **2020**, 10, 320. [CrossRef] [PubMed]
82. Gasteiger, J.; Marsili, M. A New Model for Calculating Atomic Charges in Molecules. Tetrahedron Lett. **1978**, 19, 3181–3184. [CrossRef]
83. O'Boyle, N.M.; Banck, M.; James, C.A.; Morley, C.; Vandermeersch, T.; Hutchison, G.R. Open Babel: An Open Chemical Toolbox. J. Cheminform. **2011**, 3, 33. [CrossRef] [PubMed]
84. Trott, O.; Olson, A.J. Autodock Vina: Improving the Speed and Accuracy of Docking with a New Scoring Function, Efficient Optimization, and Multithreading. J. Comput. Chem. **2010**, 31, 455–461. [CrossRef]
85. Dallakyan, S.; Olson, A.J. Small-Molecule Library Screening by Docking with Pyrx. In Chemical Biology: Methods and Protocols; Hempel, J.E., Williams, C.H., Hong, C.C., Eds.; Springer: New York, NY, USA, 2015; pp. 243–250.
86. Brooks, B.R.; Brooks, C.L., III; Mackerell, A.D., Jr.; Nilsson, L.; Petrella, R.J.; Roux, B.; Won, Y.; Archontis, C.; Bartels, G.; Boresch, S.A.; et al. Charmm: The Biomolecular Simulation Program. J. Comput. Chem. **2009**, 30, 1545–1614. [CrossRef] [PubMed]
87. Sehnal, D.; Svobodová Vařeková, R.; Berka, K.; Pravda, L.; Navrátilová, V.; Banáš, P.; Ionescu, C.-M.; Otyepka, M.; Koča, J. Mole 2.0: Advanced Approach for Analysis of Biomacromolecular Channels. J. Cheminform. **2013**, 5, 39. [CrossRef] [PubMed]
88. Dong, S.-H.; Lam, N.; Nagarajan, R.; Nair, S.K. Structure-Guided Biochemical Analysis of Quorum Signal Synthase Specificities. ACS Chem. Biol. **2020**, 15, 1497–1504. [CrossRef] [PubMed]